

Study of Two-Step Mechanisms in Pion Absorption on ${}^6\text{Li}$, ${}^{12}\text{C}$ via Deuteron Emission

G.M. Huber*, G.J. Lolos, Z. Papandreou, J. Hovdebo, S.I.H. Naqvi

Department of Physics, University of Regina, Regina, SK S4S 0A2 Canada

D.F. Ottewell, P.L. Walden

TRIUMF, Vancouver, BC V6T 2A3 Canada

G. Jones

Department of Physics, University of British Columbia, Vancouver, BC V6T 1Z1 Canada

X. Aslanoglou^(a)

Department of Physics and Astronomy, Ohio University, Athens, OH 45701-2979

(November 21, 2018)

The (π^+, pd) , and (π^+, dd) reactions were investigated with pions of 100 and 165 MeV kinetic energy on ${}^6\text{Li}$ and ${}^{12}\text{C}$ targets. In comparison with previously published (π^+, pp) data on the same targets and at the same beam energies, kinematic regions were identified in which the neutron pickup process $n+p \rightarrow d$ dominated the observed deuteron yield. The importance of this mechanism increases with energy, contributing half of the observed cross section at 165 MeV. The contribution of direct quasi-triton absorption is significant only at 100 MeV.

25.80.Ls,25.80.Hp,25.10.+s

I. INTRODUCTION

Pion absorption reactions have been studied for many years because of their importance in understanding the pion-nucleus interaction in general. Much of this effort has been spent in trying to understand the underlying pion absorption mechanism. Because of energy and momentum conservation arguments, a minimum of two nucleons in the nucleus must be involved in the pion absorption process. However, progress in understanding the answer to questions such as the relative importance of absorption mechanisms involving three or more nucleons, and the role of two-step mechanisms, has been difficult, with experiments often giving conflicting or incompatible signals.

*Corresponding Author: TEL: 306-585-4240, FAX: 306-585-5659, E-mail: huberg@uregina.ca

With few exceptions, previous experiments have concentrated on the detection of energetic protons or neutrons emitted after pion absorption. They have indicated that two-nucleon absorption is the dominant absorption mechanism at low energy ($T_\pi \approx 50$ MeV) and that its importance drops with energy, accounting for less than 40% of the absorption cross section by $T_\pi = 240$ MeV [1]. Three-nucleon absorption increases in importance with energy, and four-nucleon processes must be taken into account for nuclei as heavy as ^{12}C . Recently, LADS has also found conclusive evidence of the role of two-step mechanisms in the pion absorption process [2].

A small fraction of recent pion absorption experiments have also paid some attention to the deuterons emitted in coincidence with a proton (i.e. (π^+, pd)). These experiments have been of interest because direct absorption on a pnn cluster can be cleanly identified without recourse to error-prone extrapolations over large regions of phase-space, and because the role of a second-step final state interaction (FSI) can be studied via the nucleon pickup process $p + n \rightarrow d$. A synopsis of the most representative works follows.

An early study on ^7Li and ^{12}C was published in 1978 by Comiso et al. [3]. The effects of absorption on two nucleons were clearly visible in the Dalitz plots formed from both elements, but effects due to absorption on larger clusters could only be found in Li . In 1986, Wharton et al. [4] investigated the (π^+, pd) reaction on $^{6,7}\text{Li}$ at $T_\pi = 59.4$ MeV over a narrow angular range using a high resolution crystal spectrometer. Bound states of $^3,^4\text{He}$ dominated their excitation spectra, and they found that a model in which the pion interacts and is absorbed on a “quasi-triton” cluster described the main features of their data very well. Yokota et al. published two studies [5,6] obtained with a low resolution scintillator array. In the first, angular correlations for the (π^+, pp) and (π^+, pd) reactions on ^{nat}C at $T_\pi = 65$ MeV were compared, and it was found that the ratio $d\sigma(\pi^+, pd)/d\sigma(\pi^+, pp) \approx 0.025$ was more constant with angle than expected if the pd were due to direct three-nucleon absorption. In the second, more detailed study on $^{6,7}\text{Li}$, it was found that at $T_\pi = 165$ MeV, the (π^+, pd) angular distribution is well reproduced by the quasi-triton model at backward deuteron angles, $\theta_d > 120^\circ$, but is higher than the model by at least 300% for $\theta_d < 60^\circ$, indicating the contribution of more complicated reaction mechanisms.

More recently, the BGO Ball Collaboration published “detected” cross sections for events involving one or more deuterons in coincidence with one or more protons [7,8]. Data were obtained on ^6Li , ^{12}C , ^{27}Al , ^{58}Ni , ^{118}Sn , ^{238}U at $T_\pi = 50, 100, 150,$ and 200 MeV. They found that the angular distributions and correlations for proton and deuteron emission are similar to those of two-proton emission, suggesting that most deuteron emission is probably due to neutron pickup by protons. Bauer et al. [9] studied ppp , pd , and ppd emission following absorption of 65 MeV π^+ on ^{16}O . They found evidence for backward-peaked direct deuteron emission, confirming the finding of Yokota et

al. that deuteron emission has different signatures at forward and backward angles. Finally, the results of the LADS Collaboration are summarized by Rowntree [10]. Their experiment utilized a detector which recorded coincidences between all types of outgoing particles, charged and neutral, following π^+ absorption. With this LADS detector, which covered more than 98% of 4π , data were obtained for ${}^4\text{He}$, N , and Ar gas targets, with a detection threshold of approximately 20 MeV for protons and neutrons, and 25 MeV for deuterons. They found that deuteron emission is strongly correlated with the emission of other energetic charged (but not neutral) particles, accounting for nearly 10% of the total cross section on N when two charged particles are emitted, but approximately 50% when four or more charged particles are emitted.

In summary, previous results point to contributions from both quasi-triton absorption and neutron pickup mechanisms. While the total cross section of pion absorption leading to deuteron emission is a small fraction of the total absorption cross section, it is of particular interest because it can provide additional information concerning the more conventional pp , ppp and ppn channels. In the kinematic regions where pd emission exhibits signatures of quasi-triton (ppn) absorption, it can provide information on $T=1/2$ isospin cluster composition in the ground state of nuclear systems. The two-body nature of the pd final state may also make the extraction of such information more certain than the three-body ppn channel, whose extraction is based on three-body phase-space extrapolations.

On the other hand, the pd and dd exit channels may provide better information on the role of hard FSI (in terms of pick-up processes) than can be provided by re-scattering or other less understood types of FSI. Even though FSIs have long been recognized as one of the complications in pion absorption which can mimic multi-nucleon absorption mechanisms, such interactions have been very difficult to identify and quantify with any certainty and confidence. This problem has been partly due to the difficulty of extracting FSI signatures from the many various channels available to them, partly due to the broadening of the distributions due to the Fermi momenta of the particles involved, and partly due to the multi-body phase-space distributions that need to be unfolded and which are not unambiguous. Thus, although initial state interactions (ISI) in pion absorption have been identified and quantified (Ref. [2,11]), the clean identification of FSI remains elusive. A clear signature of FSI in terms of pick-up reactions, both qualitatively and quantitatively, will greatly assist our understanding of two-step FSI contributions in this and other hadron final-state reactions.

In this work, we present results for the (π^+, pd) and (π^+, dd) reactions on ${}^6\text{Li}$ and ${}^{12}\text{C}$ targets at 100 and 165 MeV incident pion energies. This is the final of a series of papers [12–14] resulting from a pion absorption experiment at TRIUMF.

II. EXPERIMENT AND DATA ANALYSIS

pp coincidence results following π^+ absorption on ${}^6\text{Li}$ and ${}^{12}\text{C}$ with this experimental apparatus have already been published [12–14]. These publications, as well as reference [15], describe the apparatus and data analysis in considerable detail. Therefore, the experiment will only be briefly described here, with special attention paid to those aspects of the analysis which are specific to the detection of deuterons.

The experiment was performed at the M11 pion channel at TRIUMF, using π^+ beams with kinetic energies of 100 and 165 MeV at the center of the target. Pions were identified by time-of-flight measurements, and the total incident flux was corrected for the known μ^+ and e^+ contaminations. The flux measurement was determined using a plastic scintillator counter positioned upstream of the target which was normalized to another in-beam monitor having the same size as the target and placed directly in front of it, but removed during the data taking. Typical beam rates were 3 MHz with pile-up corrections of approximately 8.5% applied.

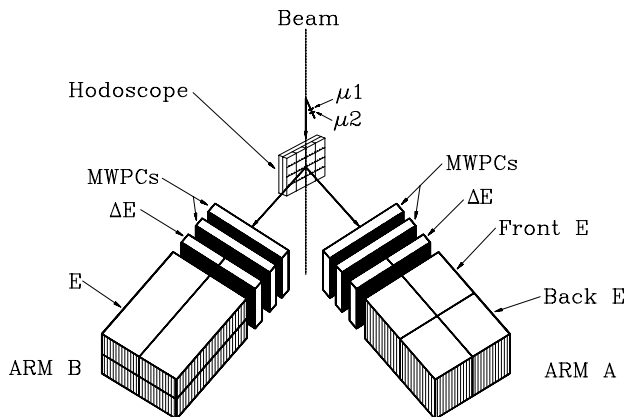


FIG. 1. Schematic diagram of the experiment. Full details of the apparatus are discussed in reference [15].

The targets, metallic ${}^6\text{Li}$ with a 95% enrichment factor, and ${}^{nat}\text{C}$ (research grade graphite), were alternately mounted on the downstream side of a segmented plastic scintillator hodoscope which measured the beam profile and acted as an extra flux monitor. As a result of the carbon content in the $(\text{CH}_{1.1})^k$ scintillator hodoscope, a carbon subtraction had to be employed to obtain the ${}^6\text{Li}$ data. The hydrogen content of the hodoscope, however, clearly did not contribute to the (π^+, pd) reaction. The areal densities of the targets were 112 mg/cm^2 for the ${}^6\text{Li}$ target, and 399 mg/cm^2 for the ${}^{nat}\text{C}$ target. The carbon content of the hodoscope contributed an additional 190 mg/cm^2 .

The scattered particles were detected in two detector arms composed of plastic scintillators and multiwire proportional chambers (MWPC), shown schematically in figure 1. The two arms were located on opposite sides of the pion

beamline, and could be rotated independently around the center of the scattering table between angles of 20° and 150° with respect to the incident π^+ beam, measured from the physical edges of the detectors. Each arm was segmented into two subassemblies (Left and Right) with respect to the incoming pion beam, with two common MWPCs in each arm, but with separate $\Delta E - E$ detectors which provided the particle identification and energy information. Arm A was equipped with four 15 cm thick blocks, each viewed by two photomultiplier tubes (PMTs) via 45° total reflection prism light guides, while Arm B consisted of four 30 cm thick monoblocks, each viewed by a single PMT. The ΔE counters were viewed by two PMTs each. This configuration resulted in a 220 MeV maximum stopping power of the detectors for protons [15], which translates to a range of 30 cm. The MWPCs provided particle trajectory information, allowing a three-dimensional traceback of each event to the target.

The trigger was defined by the four-fold coincidence $\Delta E_A \cdot E_A \cdot \Delta E_B \cdot E_B$, in any of the four possible combinations of the subassemblies, as long as one charged particle was recorded on each side of the beam. For Arm A, E_A was defined by the front E counter only, with the back E counter not included in the trigger decision. Thus, for a pair of central angles of each arm, data were collected simultaneously for four effectively independent telescope coincidence combinations. As the angular acceptance of each arm was $\Delta\theta = 22^\circ$, each coincidence combination involved 11° in each arm. Data were obtained for a variety of subassembly angle combinations between 22° and 145° on each side of the beam. The angular resolution of the reconstructed event was 1.6° , taking into account the MWPC tracking resolution of each arm and the divergence of the incident pion beam. The light output response and normalization of the detectors and electronics were calibrated and periodically monitored throughout the run via the known proton energies from the $d(\pi^+, pp)$ reaction at several proton conjugate angles at 100 and 165 MeV incident pion energies, as described in [12–14].

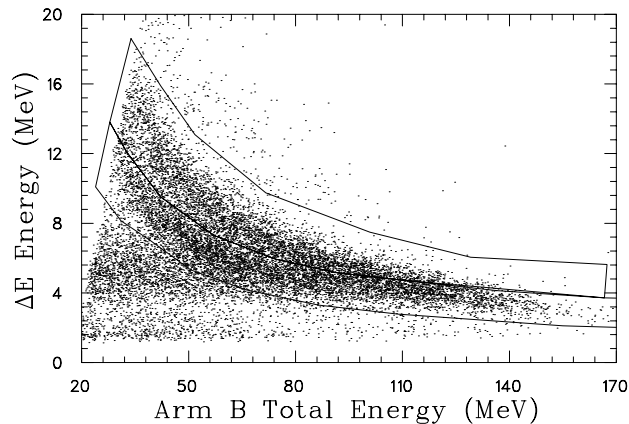


FIG. 2. A representative particle identification plot from the experiment. Bands due to proton and deuteron emission are clearly visible.

A representative particle identification (PID) plot is shown in figure 2, showing that pions and/or muons, protons, and deuterons were clearly separated. In Arm A, energetic protons penetrating the front counters and stopping in the rear counters formed additional PID bands, providing a greatly enhanced separation of pions and/or muons from the protons. In addition to the periodic $d(\pi^+, pp)$ runs, the gain stability of each detector was verified for the data obtained at each angle pair setting by checking to make sure that the proton band remained at its calibrated position. The offline software gain parameters were occasionally adjusted as needed.

Particles located within the upper and lower boxes of figure 2 were identified as deuterons, and protons, respectively. Events which fall far to the left of the proton band correspond to particles which either suffered nuclear reactions in the detector (“reaction losses”) or did not stop in the detector due to the initial trajectory or multiple scattering (“edge effects”). Energy-dependent corrections were made for these effects, based on the ratio of events to the left of the proton band to the number of events in the proton band. This correction is described in more detail in reference [14]. Typical factors, for the energy region of highest population (135 to 165 MeV), are 1.20 to 1.35, respectively. No reaction loss correction was applied to deuterons as there was no independent method of determining its value.

It has been shown that the light output versus energy deposition depends on whether the particles were traversing or stopping in the scintillators [16]. For arm A, where the thick front blocks could either stop protons or allow them to be transmitted to the rear blocks, such differences in light output were readily observed and easily corrected for. These corrections were compared to the well-defined proton energies expected from the $d(\pi^+, pp)$ reaction, and were found to be in excellent agreement. An additional correction was applied to the light output from the stopping counter if the particle was identified as a deuteron, in order to adjust for the difference in the light output of the deuteron relative to the proton because of the different ionization density and subsequent quenching in the scintillators. The light output curve was parameterized by a quadratic polynomial and an exponential equation according to the light output data provided in reference [17].

Instrumental energy resolutions of 2.9% and 2.6% (σ) at incident pion energies of 100 and 165 MeV, respectively, were achieved, once all corrections were made. These numbers translate to approximately 4 MeV (σ) for the resolution in the excitation spectra. A uniform detection threshold of 45 MeV for protons, and 50 MeV for deuterons was imposed to avoid threshold variations resulting from the different target angle orientations and the associated variation in the energy loss in the target. MWPC efficiencies, determined on a run-by-run basis and in a cyclic manner for each MWPC, were also applied to the data.

Finally, the geometrical solid angle of each two-arm coincidence-pair was corrected for the effects of multiple

scattering, finite beam spot size, and limited vertical acceptance, by implementing an acceptance correction factor

$$d\Omega_1 d\Omega_2_{expt} = d\Omega_1 d\Omega_2_{point} * Acc,$$

where $d\Omega_1 d\Omega_2_{point}$ are the point source solid angles of the front face of the E counters in each arm subassembly consistent with the data analysis. The factor Acc (equal to 0.80 ± 0.07 at both incident pion energies) was determined using a Monte Carlo in which three-energetic emerging body phase space is assumed for the out-of-plane distribution. After application of this factor, the experimental data may be reliably integrated over 4π .

III. MONTE CARLO MODELS

A. Motivation

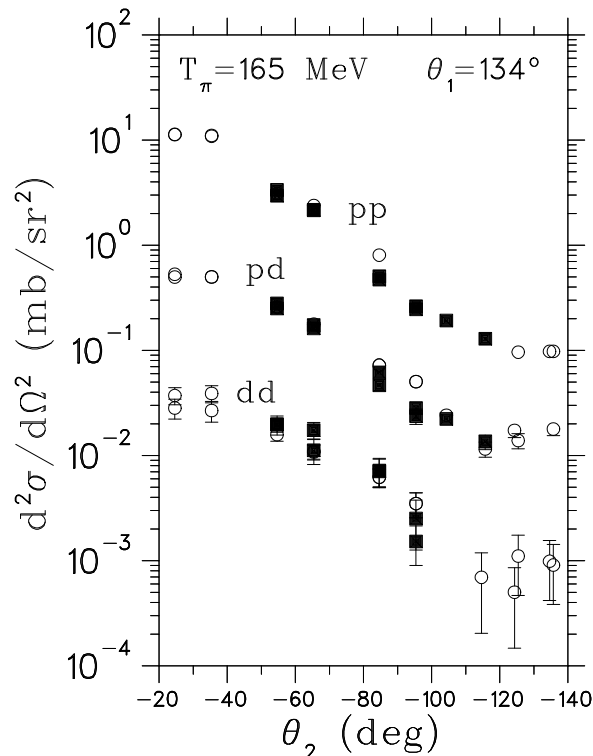


FIG. 3. The open circles are ^{12}C and the filled squares are 6Li target, respectively. It should be emphasized that the angular distributions are not arbitrarily offset from each other, but reflect the actual cross sections for each process.

Representative angular distributions of the data are shown in figure 3. Two striking features emerge. The first is that the angular distributions for the pp , pd and dd final states are nearly identical in shape, with the pd distribution slightly flatter than the pp distribution, and the dd distribution the flattest of all. This similarity was reported earlier

for pd emission from a variety of nuclei by Ransome et al. [8] who concluded “that most deuteron emission is probably due to neutron pick-up by protons”. Unfortunately, however, the poor angular resolution of the BGO Ball data did not allow this hypothesis to be tested in a more quantitative manner. The even flatter angular distribution characteristic of dd emission is a new observation, and serves to reinforce the argument for the prevalence of neutron pickup. In the case of figure 3, the decrease in cross-section as θ_2 varies from -25° to -145° is a factor of 150 for pp , 42 for pd , and only 16.5 for dd .

The second significant feature of figure 3 is that the differential cross section is reduced by nearly the same factor of ten between pp and pd as between pd and dd , regardless of whether the emission is from ${}^6\text{Li}$ or ${}^{12}\text{C}$. This is especially noteworthy, because the dd reaction on ${}^6\text{Li}$ leaves no remaining neutrons, while the reaction on ${}^{12}\text{C}$ leaves three unobserved neutrons, and so the two reactions must have significantly different neutron pickup combinatorics.

The extent to which neutron pickup could account for the nearly constant factor between the different angular distributions can be obtained from a rough estimate based on the total cross section (approximately 15 mb [18–20]) for the ${}^{12}\text{C}(p, d){}^{11}\text{C}_{g.s.}$ process between $T_p = 30$ and 65 MeV. If we naively assume that the π^+ absorption occurs in the center of the ${}^{12}\text{C}$ nucleus, we immediately obtain a $p + n \rightarrow d$ pickup probability of 4.6%. So, it is conceivable that a full calculation could account for a large portion of the 10% deuteron emission probability observed in figure 3. To study this in more detail, two Monte Carlo simulations were employed. These are described below.

B. $p + n \rightarrow d$ pickup

This model simulates the production of a deuteron by pion absorption on ${}^{12}\text{C}$ under the assumption that the absorption initially leads to the emission of nucleons: two protons, which are tracked in the simulation, and any remainder which are handled through appropriate setting of the missing momentum and mass variables. One of the protons combines with a neutron to form the deuteron observed in the final state, while the other proton continues to the detectors. The effect of the various absorption mechanisms at the initial absorption vertex, such as the absorption on two, three or four nucleons, or soft initial- or final-state interactions, are taken into account in an empirical manner via the method discussed below.

The CERN program, GENBOD [21], was used to create the momentum vectors of the participating particles, two protons, one neutron, and recoiling excited ${}^9\text{B}$, randomly chosen within the available phase-space of the reaction. To account for the various possible absorption mechanisms leading to extra unobserved nucleons, a triple-differential cross section for the events was employed, parameterized from the 100 and 165 MeV ${}^{12}\text{C}(\pi^+, pp)$ data of reference

[14]. To simplify matters, the differential cross section was assumed to be separable into functions over angle and excitation energy

$$\frac{d^3\sigma}{d\Omega_{p_1}d\Omega_{p_2}dE_{exc}}(T_\pi, \vec{p}_{p_1}, \vec{p}_{p_2}) = \frac{d^2\sigma}{d\Omega_{p_1}d\Omega_{p_2}}(T_\pi, \theta_{p_1}, \theta_{p_2}) \cdot \frac{dS}{dE_{exc}}(T_\pi, p_{p_1}, p_{p_2}, \Delta\theta_{QFA}), \quad (1)$$

where $\frac{dS}{dE_{exc}}$ refers to the normalized excitation energy spectra for pp emission, and $\Delta\theta_{QFA}$ is the difference between the second detected particle angle and the angle expected from simple $d(\pi^+, p)p$ kinematics. All other variables are standard, and should be self-explanatory.

For several values of the first proton angle, the $^{12}C(\pi^+, pp)$ angular distributions, $\frac{d^2\sigma}{d\Omega_{p_1}d\Omega_{p_2}}$, were fit over the second proton angle with the sum of two Gaussians, one narrow and one broad, both having the same centroid. The individual coefficients of this fit were then parameterized in terms of Legendre polynomial functions of the first proton angle. The cross section for a particular event could then be calculated, at pion energies of 100 MeV or 165 MeV, in terms of the scattering angles of the two protons. The choice of function for these fits was based purely on achieving a good fit with few variables, and is not meant to imply any additional physical significance.

The parameterization of $\frac{dS}{dE_{exc}}$ was based on the normalized excitation energy spectra for proton emission from reference [14]. The shape of the excitation energy spectra is a function of the angle difference between the observed second proton angle and the angle expected from simple $d(\pi^+, p)p$ kinematics, $\Delta\theta_{QFA}$. At zero difference between the angles, there is a prominent peak for low excitation, due to the large contribution from direct absorption on two protons, with the spectrum falling off rapidly thereafter. As the difference increases further, a broader distribution due to contributions from processes involving more nucleons becomes part of the spectrum. This addition causes a smearing of the two-proton absorption peak, giving the distribution an overall Gaussian shape with center at higher excitation energies. The spectra were thus fit using a piecewise function consisting of a Gaussian definition that gives way to a linear term. By varying the parameters of this function, including the point where the definition of the function switches from Gaussian to linear, the spectra could be fit quite well with the same function for all values of the angular difference.

The simulation then assumed that one of the protons picked up a neutron, via a hard final-state interaction, to form the deuteron observed in the final state. The pickup of the neutron by a proton in the recoil nucleus was approximated by the experimentally measured differential cross sections for the reaction $^{12}C(p, d)^{11}C_{g.s.}$ as a function of T_p, θ_d [18–20, 22–24], after appropriate Lorentz transformation to the c.m. frame of the struck neutron, $^9B^*$ system. This nucleus was chosen, rather than ^{10}B , because of the availability of experimental data. Comparison with the limited ^{11}B data available indicate that this approximation should affect the model in any significant manner. As

the cross section for the $^{11}C_{g.s.}$ final state is an order of magnitude higher than for any of the other possible discrete final states, it was sufficient to use just the ground state in the Monte Carlo. The angular distributions of differential cross sections $\frac{d\sigma}{d\Omega_d}$ were fit with a sum of two Gaussians and a linear term. The fit coefficients were then obtained as a function of incident proton energy. Since the parameterization was based on (p, d) cross sections from $T_p = 30$ to 185 MeV, it did not include the ‘soft’ 1S_0 FSI, which dominates for relative NN momenta less than 80 MeV/c.

Monte Carlo data were generated with statistical weight

$$w = \sqrt{\frac{d^3\sigma}{d\Omega_{p_1}d\Omega_{p_2}dE_{exc}}(T_\pi, \vec{p}_{p_1}, \vec{p}_{p_2}) \frac{d^2\sigma}{d\Omega_d dE_{p_2}}(\vec{p}_{p_2}, \vec{p}_n, \vec{p}_d)}$$

and were then tracked through the target and detector assemblies, taking into account the effect of detector acceptance and resolution. Finally, the simulated data were analyzed in the same manner as the experimental data.

dd emission following π^+ absorption was similarly modeled via two pickup reactions. In this case, the initial input to GENBOD was modified so that five particles were produced, two protons, two neutrons and a residual 8B nucleus. The simulation then proceeded as before, but with each proton picking up a neutron to form the deuterons observed in the final state.

C. “pp-like” pd emission

What we term pp -like pd emission was simulated in the following manner. GENBOD was used to create the momentum vectors of three outgoing particles, p , d , and $^9B^*$. It was assumed that the triple differential cross section for this process is given by the same parameterization as equation (1) above, after accounting for modification due to the different phase-space characterizing the pd^9B^* final state, instead of $pp^{10}B^*$. This simulation differs from the quasi-triton $\pi^+t \rightarrow dp$ process because it incorporates the contribution of more complex reaction mechanisms present in the pp emission data. Thus, the d could either originate directly from the absorption vertex, or via knockout before absorption (ISI), or via an outgoing nucleon soft FSI which does not materially affect the outgoing momentum distributions.

Although the two mechanisms B and C, overlap somewhat kinematically, their respective energy and angle signatures are distinctive enough to allow their relative contributions to be distinguished. The comparison of the pickup and pp -like models, therefore, provides a measure of the hard neutron pickup contribution, where the momentum of the deuteron differs substantially from that of the originally emitted nucleon. Because these models are based upon empirical data, it is only possible for us to compare their relative cross sections, and not their amplitudes. Therefore,

interferences between the two mechanisms are not taken into account in our analysis. Since spin averaging and other similar effects are likely to wash out such amplitude interference effects, an argument can be made that this necessary approximation employed will not greatly affect the conclusions of the analysis.

IV. FEATURES OF THE DATA

Using these two models, it was possible to obtain a remarkably good description of all observables extracted from the data at 100 and 165 MeV pion energies incident upon ^{12}C . Because each model incorporated empirical fits to $^{12}\text{C}(\pi^+, pp)$ data, neither model was applied to the ^6Li target data. There were a number of reasons for this restriction. Firstly, a target subtraction was required to extract the ^6Li data (section II), so it is of poorer quality than the ^{12}C data. Secondly, the significant contributions of both the discrete and continuum final states make the excitation spectra for ^6Li more difficult to parameterize than the smooth distributions obtained with a ^{12}C target. Finally, because either one or zero neutrons are left unaccounted for after the reaction on a ^6Li target, the neutron momentum distributions may not be independent of each other, resulting in additional complications for the pickup model. These considerations led to an easier application of the pickup mechanism model to ^{12}C than to ^6Li . Nonetheless, the similarity of the results for the two nuclei, as shown in figure 3, lead us to believe that the conclusions drawn from the ^{12}C data will be largely applicable to the ^6Li data as well. While each model is based on a number of assumptions and simplifications, the conclusions are based primarily on kinematic distributions which tend to be relatively insensitive to details of the reaction mechanism.

A. $T_\pi = 165$ MeV data

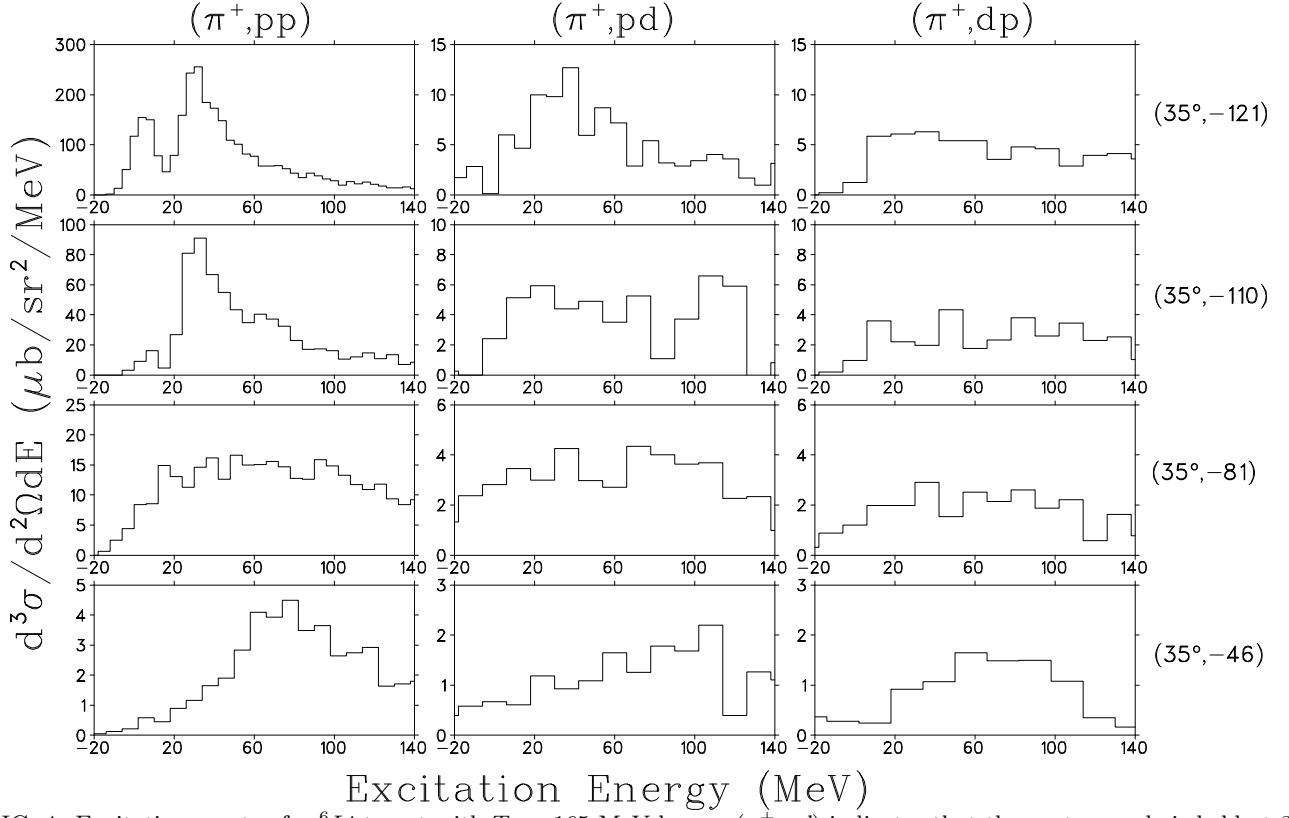


FIG. 4. Excitation spectra for ${}^6\text{Li}$ target with $T_\pi = 165$ MeV beam. (π^+, pd) indicates that the proton angle is held at 35° while the deuteron angle is scanned on the other side of the beam, while (π^+, dp) indicates the reverse. From top to bottom, the rows of histograms correspond to $\Delta\theta_{QFA} = 4^\circ, 15^\circ, 44^\circ$ and 79° , respectively.

To discern the contribution of neutron pickup to the observed deuteron yield, we first examine the excitation spectra. In our earlier publications [13,14], we noted that the single most important determinant of the (π^+, pp) excitation spectra of ${}^6\text{Li}$ and ${}^{12}\text{C}$ was the difference in angle setting between the two arms and that of $\pi^+d \rightarrow pp$ kinematics, $\Delta\theta_{QFA}$. Close to quasi-free absorption kinematics, $\Delta\theta_{QFA} \approx 0$, the pp excitation spectra exhibited bound state peaks at low excitation due to the direct emission of protons following pion absorption. At $\Delta\theta_{QFA} \geq 30^\circ$, evidence of more complex mechanisms (greater than two-nucleon absorption and multi-step processes), were more apparent. These features are repeated in the left columns of figures 4 and 5.

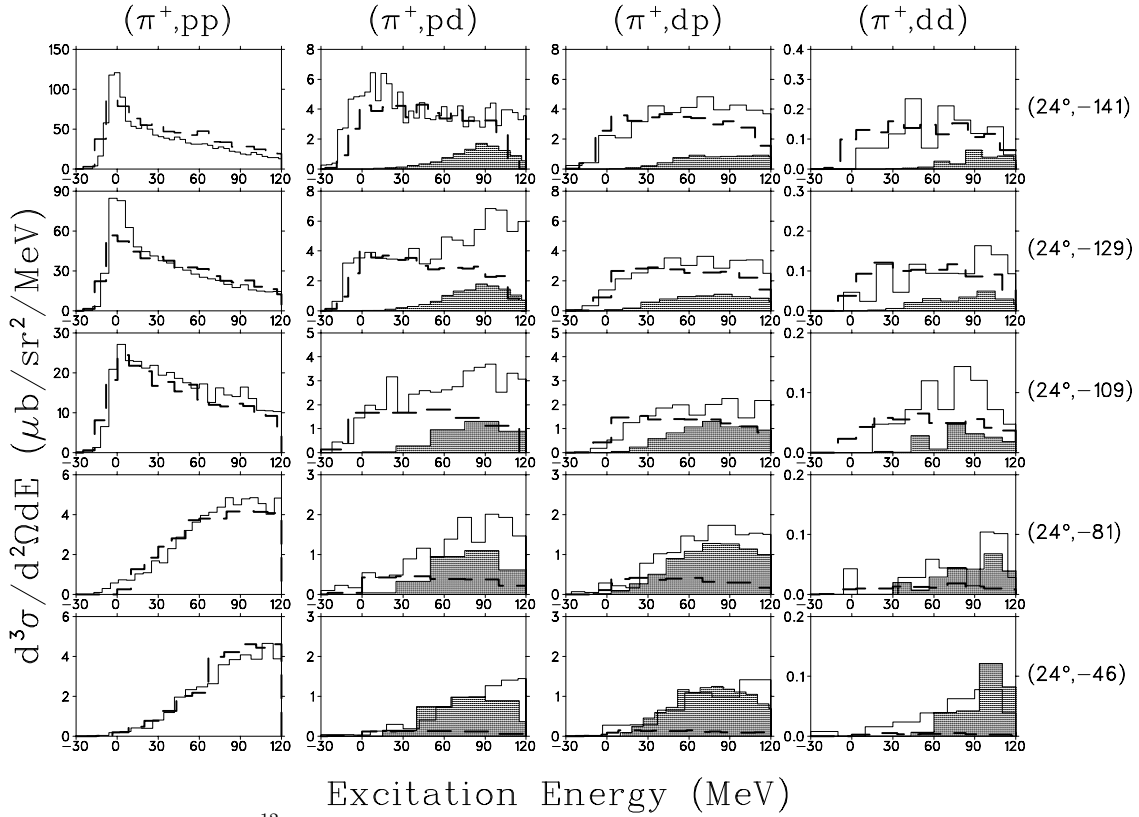


FIG. 5. Excitation spectra for ^{12}C target at $T_\pi = 165$ MeV. From top to bottom, the rows of histograms correspond to $\Delta\theta_{QFA} = 1^\circ, 13^\circ, 33^\circ, 61^\circ,$ and 96° , respectively. The solid lines are the experimental data, while the dashed lines on the left column are the parameterization of the pp excitation spectra used as input to the pd and dd models. On the three columns on the right, the dashed lines indicate the contributions of the pp -like model, and the shaded regions are those of the pickup model. All curves associated with a given model incorporate the same 165 MeV normalization.

The dependence of the (π^+, pd) excitation spectra on $\Delta\theta_{QFA}$ is much weaker than for (π^+, pp) . With the aid of the two models, this weaker dependence can now be understood. Figure 5 indicates that the contribution of the pp -like model falls rapidly as one scans away from quasi-free kinematics (i.e. moves from the top to the bottom of the figure). However, the contribution of the neutron pickup mechanism remains more constant with angle, and accounts for essentially all of the deuteron yield at $\theta_1 = 24^\circ, \theta_2 = -46^\circ$. The sum of the two models provides an excellent description of the data. These conclusions also apply to the (π^+, dd) data. It should be noted that the modeled pickup reaction is highly non-quasi-free in nature, and so contributes to the $E_{exc} > 50$ MeV region, which corresponds to lower emitted deuteron energy. The contribution of ‘soft’ neutron pickup may be included in the low excitation region covered by the pp -like model.

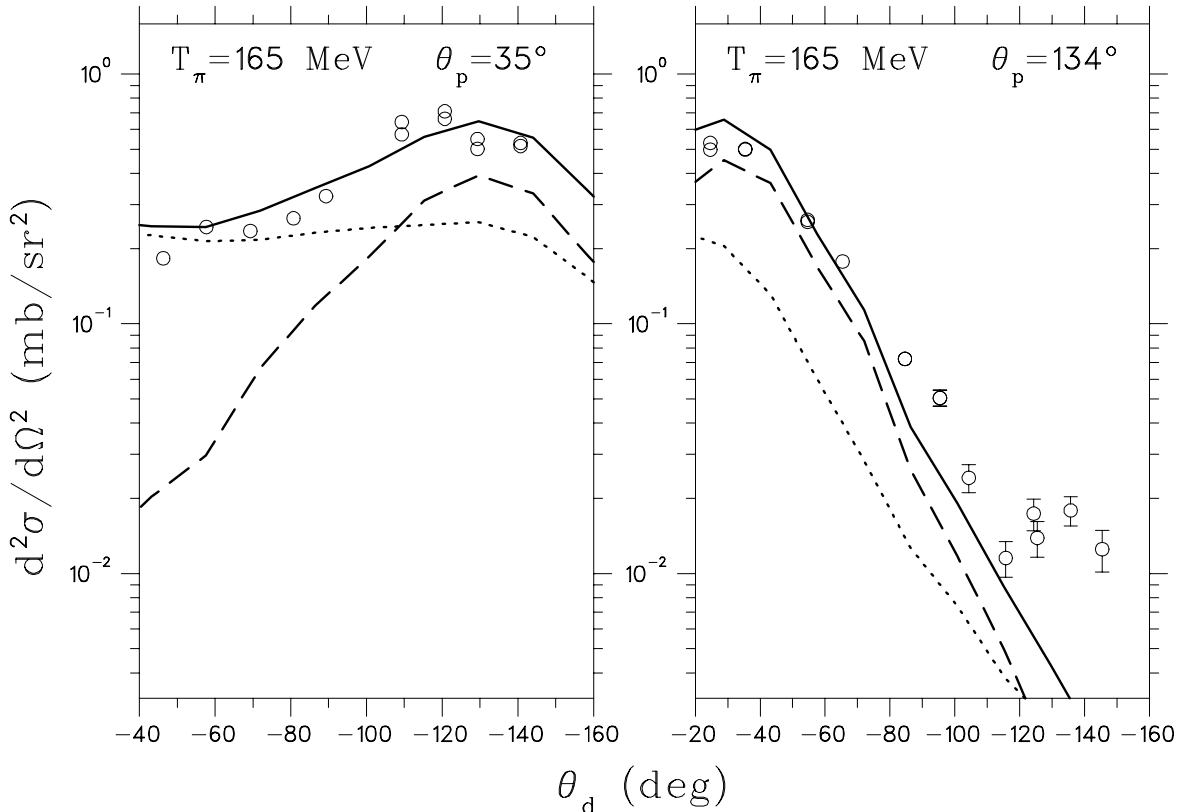


FIG. 6. Angular distributions of the $^{12}\text{C}(\pi^+, pd)$ data at 165 MeV, for the proton angle held constant at the value indicated, and the deuteron scanned on the opposite side of the beam. The dashed curves are the contributions of the pp -like model, the dotted curves the contributions of the pickup model, and the solid curve the sum of the two. The same normalization factors are used for both panels, and are the same as for the corresponding models in figure 5.

The role of the neutron pickup mechanism is perhaps shown more clearly in figure 6. Because the $pn \rightarrow d$ process is strongly forward peaked, it leads to a significant difference between the angular distributions of forward angle and backward angle deuteron emission. In both cases, the observed deuteron yield due to neutron pickup is the convolution of two factors: the distribution characteristic of the originally exiting protons, given approximately by the dashed curve in both panels, and the $pn \rightarrow d$ angular distribution, which is forward peaked in the rest frame of the struck neutron. For the leftmost panel, these two factors lead to an almost constant pickup contribution with deuteron angle, and a very flat (π^+, pd) angular distribution. This is consistent with the contributions shown in figure 5. In the right panel of figure 6, however, the two factors work in concert, and the neutron pickup contribution falls nearly as fast with angle as the pp -like emission model does. The contrast between the two experimental angular distributions shown here is larger than for the equivalent pp emission distributions shown in reference [14].

In summary, a significant neutron pickup contribution is observed in the ^{12}C data at 165 MeV, accounting for

nearly all of the deuteron yield when both proton and deuteron are detected at forward angles. This contribution corresponds to relatively large ${}^9B^*$ excitation. For all other angle combinations, the pickup contribution is smaller than that of the pp -like emission model. This more detailed description is consistent with the earlier findings of reference [6].

B. $T_\pi = 100$ MeV data

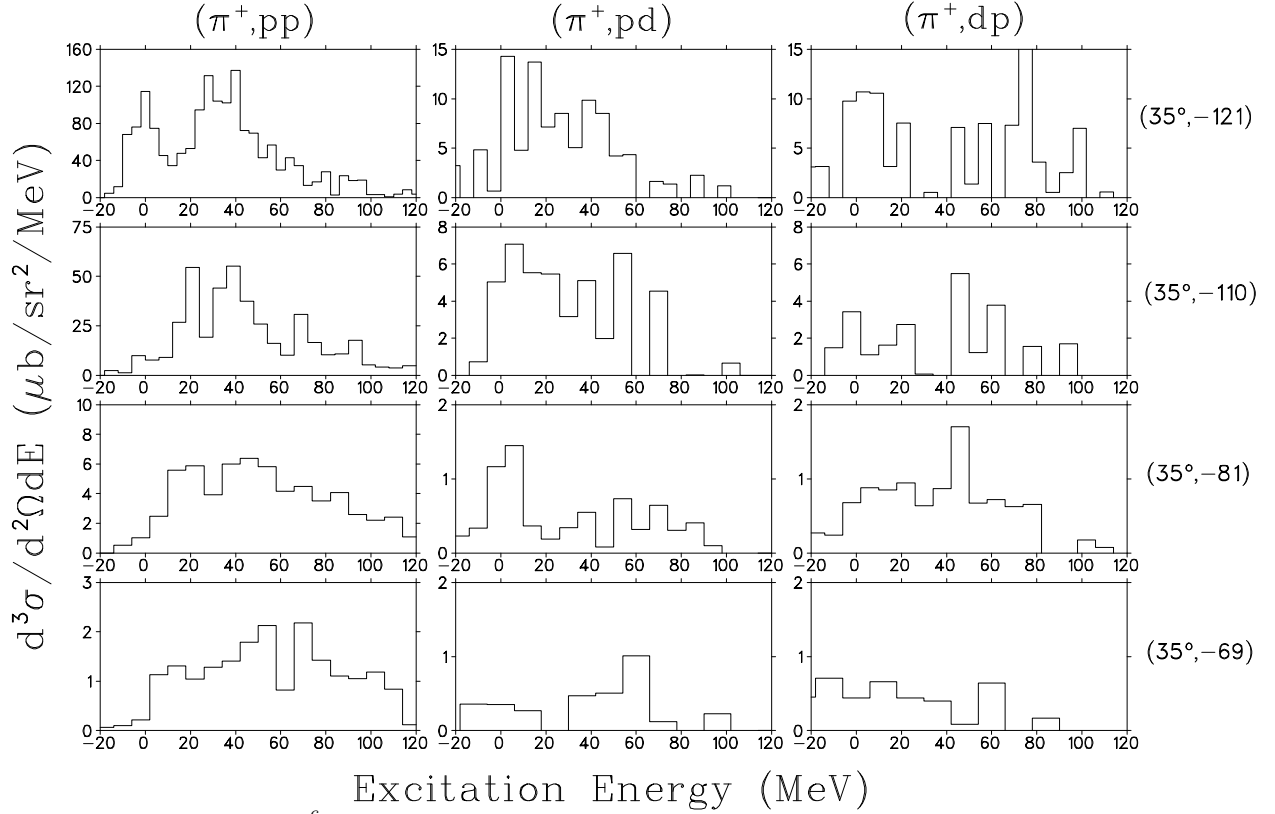
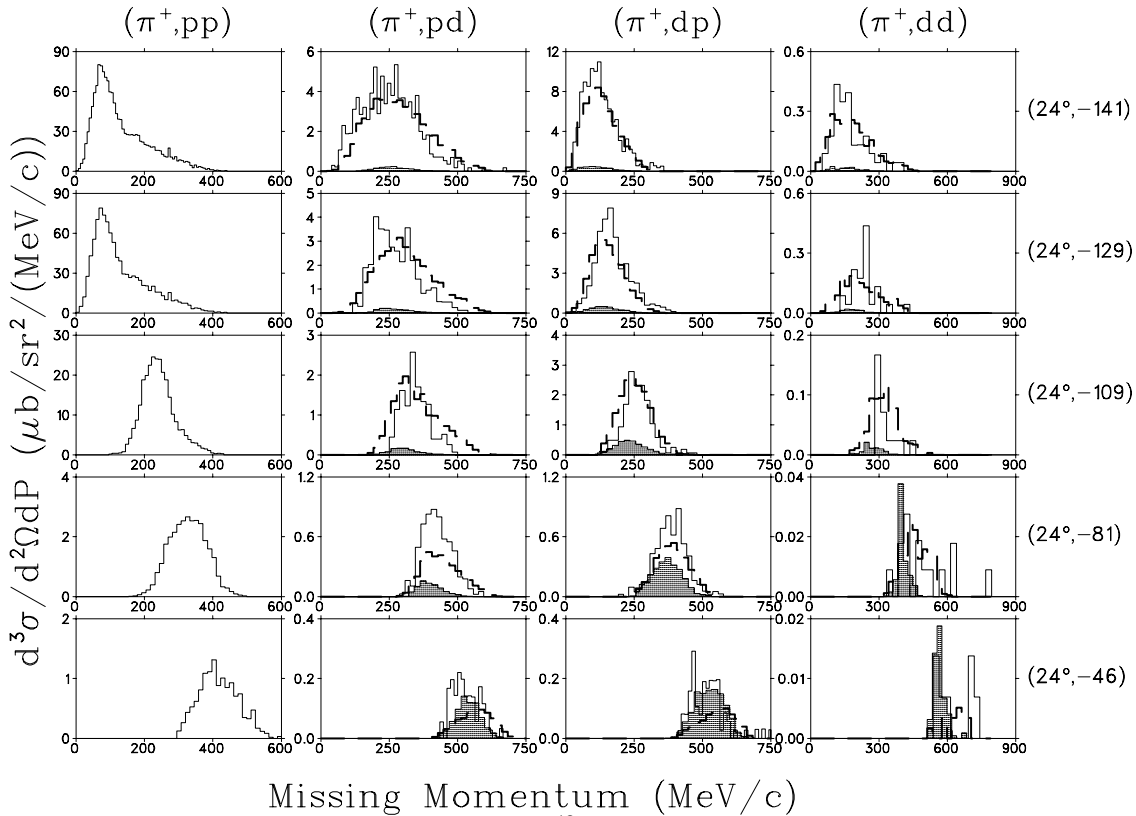


FIG. 7. Excitation spectra for ${}^6\text{Li}$ target with $T_\pi = 100$ MeV beam. From top to bottom, the rows of histograms correspond to $\Delta\theta_{QFA} = 8^\circ, 19^\circ, 48^\circ$ and 60° , respectively.

As noted in the introduction, the presence of a pronounced ground state peak in the ${}^6\text{Li}(\pi^+, pd)$ spectrum at $T_\pi = 59.4$ MeV [4] was interpreted as evidence of quasi-triton absorption. Examination of the right two columns of figures 4, 7 shows that the zero excitation region is slightly more enhanced at $T_\pi = 100$ MeV than 165 MeV, possibly indicating a small quasi-triton contribution to the reaction on ${}^6\text{Li}$ at 100 MeV. Integrating the center column data of figure 7 over all θ_d , the -20 to +20 MeV excitation region accounts for $37 \pm 7\%$ of the observed differential cross section, while the integral for the center column of the 165 MeV results (figure 4) accounts for only $14 \pm 2\%$. A similar enhancement exists for ${}^{12}\text{C}$, with the equivalent fractions being $36 \pm 7\%$, and $15 \pm 3\%$ at 100 MeV and 165 MeV,

respectively.



Missing Momentum (MeV/c)

FIG. 8. Missing momenta spectra for $T_\pi = 100$ MeV and ^{12}C target, with θ_1 held at 24° and the second arm scanned as noted. The model line types are as in figure 5, and all curves associated with a given model incorporate the same 100 MeV normalization. From top to bottom, the rows of histograms correspond to $\Delta\theta_{QFA} = 4^\circ, 17^\circ, 37^\circ, 65^\circ,$ and 100° , respectively.

A comparison of the ^{12}C models and data for the missing momentum spectra is shown in figure 8. The histograms for d emission final states have consistently higher average missing momenta than the (π^+, pp) data. However, since excitation energies of even several hundred MeV are small compared to the mass of the residual nuclear system, and thus influence the momentum of the recoiling system only slightly, the distributions of the two reaction mechanisms overlap substantially for all angle pairs, making the variable a relatively insensitive indicator. Nonetheless, the sum of the models does an excellent job of describing the pd , dp and dd emission data for all angle pairs, with the same, consistent normalization applied. Generally, the behavior is similar to that seen at 165 MeV, i.e. dominance of d knockout close to the quasi-free angle, and dominance of $p + n \rightarrow d$ pickup when both arms are at forward angles.

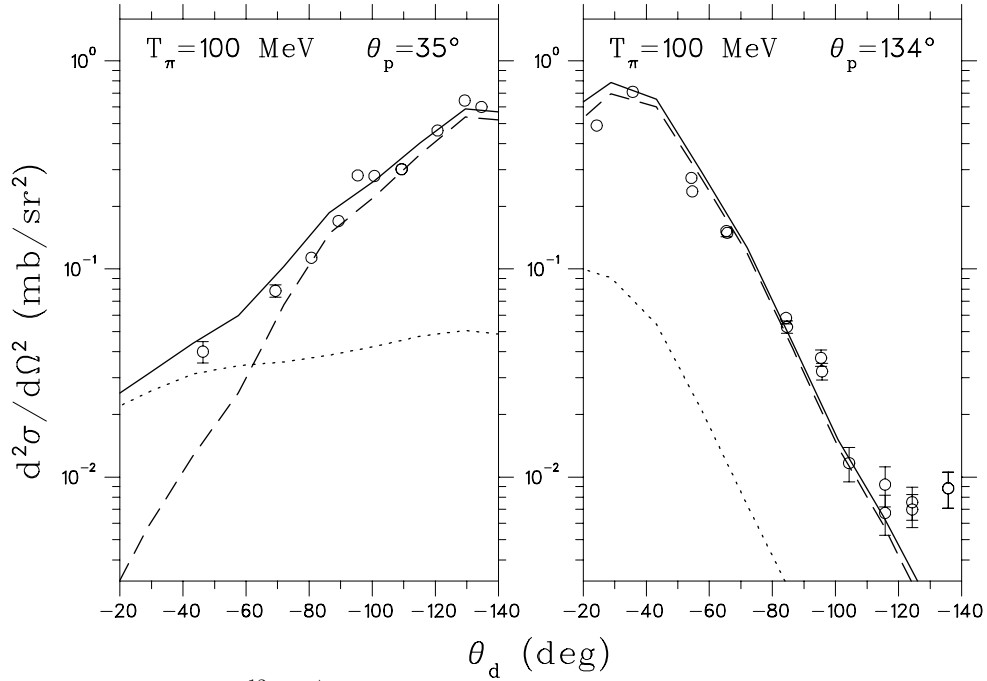


FIG. 9. Angular distributions of the $^{12}\text{C}(\pi^+, pd)$ data at 100 MeV. The curves are as in figure 6. The same normalization factors are used for both panels, and are the same as for the corresponding models in figure 8.

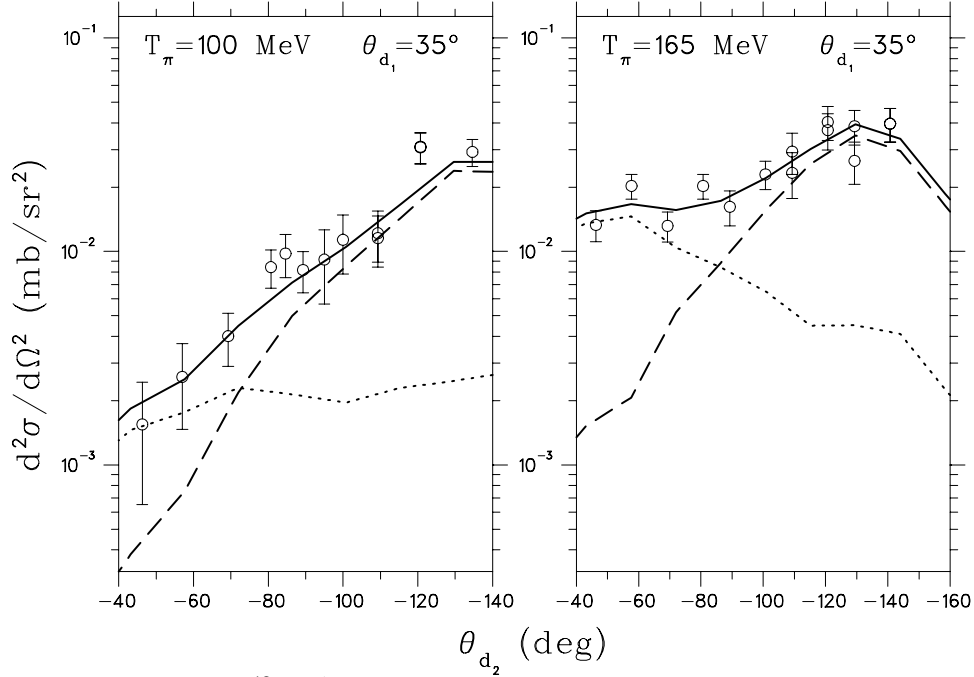


FIG. 10. Angular distributions of the $^{12}\text{C}(\pi^+, dd)$ data. The curves are as in figure 6, with the same normalization factors as used in the right columns of figures 8, and 5.

The difference in the role of the two reaction mechanisms is shown more clearly in figures 9, 10. Comparing with figure 6, as the second detector is scanned away from the quasi-free angle, the angular distributions fall more rapidly

at 100 MeV than at 165 MeV. This is due to the smaller role of the pickup mechanism at 100 MeV, a finding consistent with domination of the quasi-triton mechanism at 59.5 MeV incident pion energy [4]. However, because the cross section of the $^{12}\text{C}(p, d)^{11}\text{C}_{g.s.}$ reaction falls with energy, from 16 mb at $T_p = 30.3$ MeV, to 1.5 mb at $T_p = 156$ MeV [18,23], the argument can be made that the neutron pickup contribution should also fall with increasing incident pion energy. The observed, opposite behavior is almost certainly due to the greater multiplicity of the reaction at the higher pion energy [10]. It should be noted that the effect of the significant experimental detection threshold does not change this result in any substantive manner. Since the neutron pickup events are characterized by a relatively high excitation energy, and hence lower deuteron energy, these events suffer from the experimental threshold more severely, with a detection acceptance less than half that of the pp -like events. While both mechanisms have higher acceptances at 165 MeV than at 100 MeV, the n pickup acceptance is lower by only an additional 17% relative to the pp -like events.

In summary, the experiment indicates a larger direct quasi-triton absorption component to the reaction at 100 MeV compared to 165 MeV. Conversely, the contribution of the hard neutron pickup process is smaller at this energy.

C. Single differential and total cross sections

The double differential cross sections were fitted with Legendre polynomials and integrated in order to obtain $d\sigma/d\Omega$. Checks were made to ensure that the result was not sensitive to the highest order employed in the fits. Figure 11 displays the resulting single differential cross section angular distributions.

At both 100 and 165 MeV, the forward angle differential cross sections on ^6Li exceed those on ^{12}C , and the angular distribution has a large $30^\circ/90^\circ$ cross section ratio, resembling that of the $\pi^+d \rightarrow pp$ reaction. The figure also shows the estimated neutron pickup contribution for ^{12}C , plotted versus proton emission angle. The angular distribution of the neutron pickup contribution is especially forward peaked in the ^{12}C 165 MeV panel, and if it were subtracted from the total $^{12}\text{C}(\pi^+, pd)$ distribution (solid curve), the result would be an angular distribution more similar in shape to the ^6Li distribution. The neutron pickup mechanism contributes approximately 50% of the pd total cross section on ^{12}C at 165 MeV, but only 20% at $T_\pi = 100$ MeV.

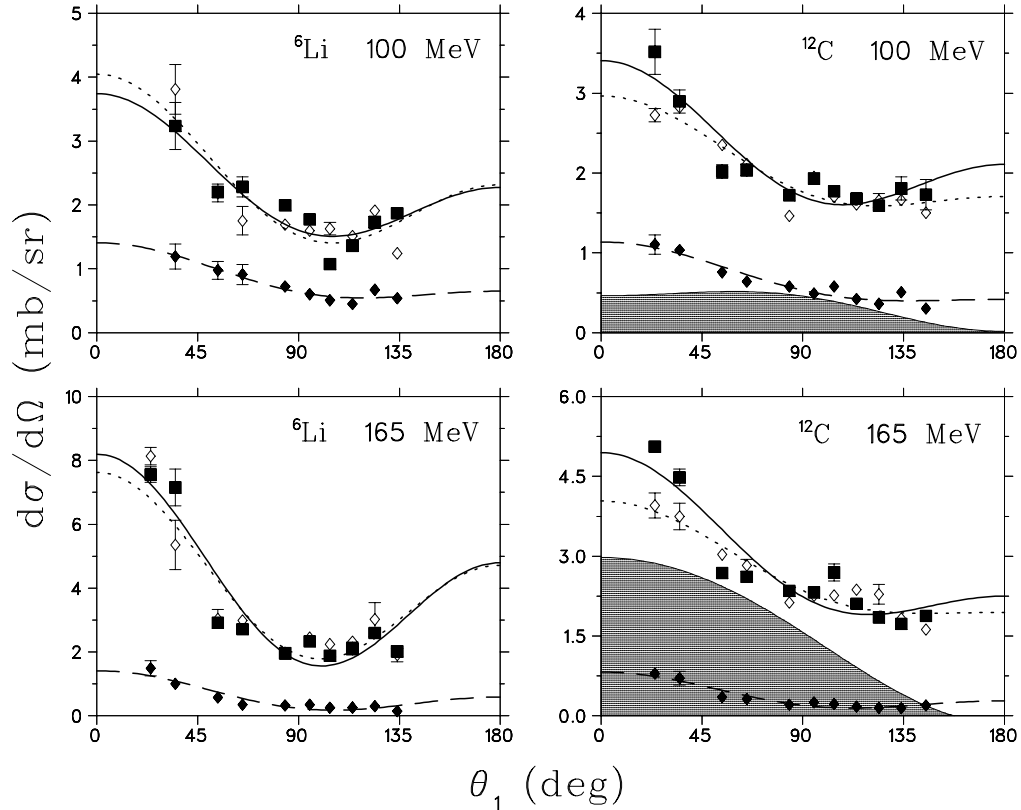


FIG. 11. Lab frame differential cross sections for the (π^+, pd) [solid squares] and (π^+, dp) [open diamonds] reactions on ${}^6\text{Li}$ and ${}^{12}\text{C}$. The solid [dotted] line is a second order Legendre polynomial fit to the (π^+, pd) [(π^+, dp)] angular distributions while the shaded regions are the estimated neutron pickup contributions, all plotted versus θ_p and to be compared against the solid curves. Finally, the solid diamonds are (π^+, pd) differential cross sections with the final state excitation restricted to 0 ± 20 MeV. These cross sections do not include contributions below the detection threshold of the experiment.

Direct quasi-triton absorption should contribute primarily to the $+20$ to -20 MeV excitation region, and so data restricted to this region are also shown in the figure. The Legendre polynomial integrated results over all angles indicate that this excitation region accounts for $37 \pm 6\%$ and $14 \pm 4\%$ of the total pd cross section on ${}^6\text{Li}$ at 100 and 165 MeV, respectively, and $30 \pm 4\%$, $12 \pm 3\%$ on ${}^{12}\text{C}$. Using $T_\pi = 65$ MeV pions on ${}^{16}\text{O}$ target, Bauer et al. [9,25] reported a significantly different angular distribution for the (π^+, pd) reaction than the (π^+, pp) reaction. While the pp events exhibited the typical $\cos^2\theta$ dependence known for quasi-deuteron absorption, the pd events had a highly asymmetric distribution, with forward-going protons and backward-going deuterons being the most likely combination. This was explained in terms of direct $\pi^+t \rightarrow pd$ absorption. In our case, the dotted and dashed curves of each panel are very similar, indicating that the proton and deuteron emission distributions are essentially identical. This reinforces the conclusion that the quasi-triton absorption component of the reaction is relatively small.

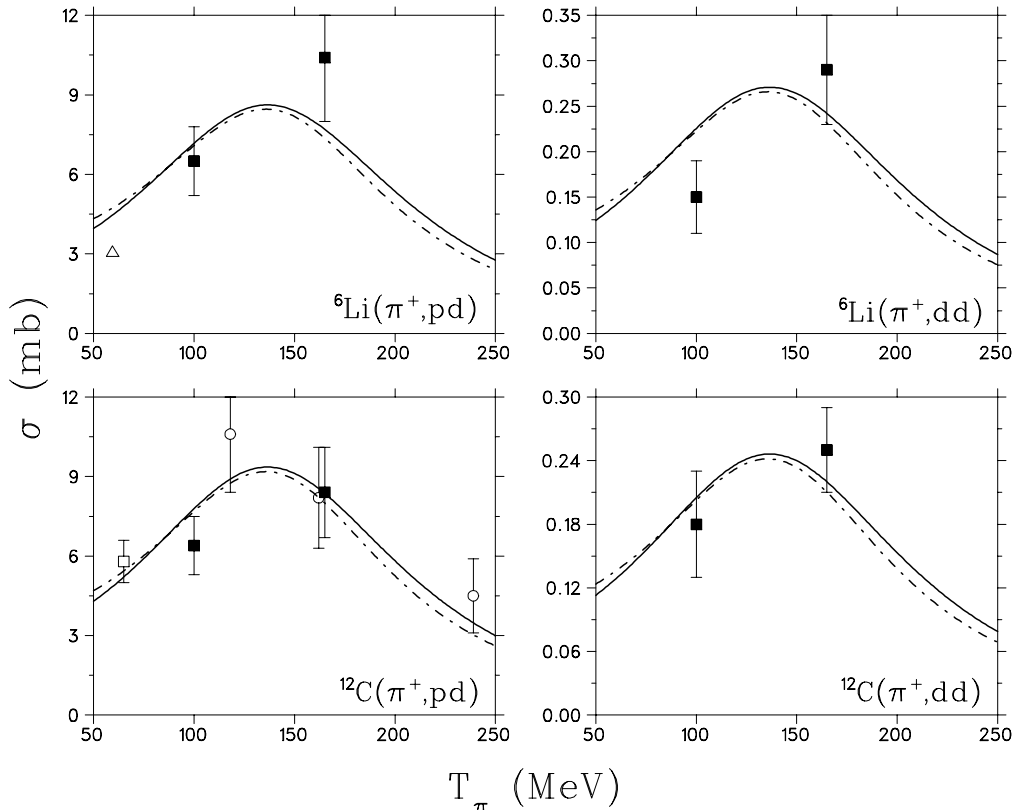


FIG. 12. Total cross sections for this work (solid squares), to discrete states of ${}^3\text{He}$ only [4] (triangle), on ${}^{16}\text{O}$ [9] (empty square), and on ${}^{14}\text{N}$ [10] (circle), the latter two scaled by $A^{2/3}$ to ${}^{12}\text{C}$ equivalent. The error bars for this work include all statistical and systematic uncertainties. In the case of the Ref. [10] results, the value shown is the sum of their “2 charged multiplicity” cross section for 1 deuteron and any number of neutrons detected, since neutrons are undetected by our apparatus. The solid curve is the parameterization of the $\pi^+d \rightarrow pp$ reaction provided by Ritchie [26], while the dash-dot curve is the parameterization by VerWest and Arndt [27]. From upper left to lower right panel, the curves are normalized by factors of 0.70, 0.022, 0.76, and 0.020, respectively.

(π^+, pd) and (π^+, dd) total cross sections were obtained by fitting the single differential cross sections with the Legendre polynomial distributions shown in figure 11, to yield the values shown in figure 12. This is the same method as used in our earlier publications [13,14] and does not include corrections for final state interactions. It is evident that the pd total cross sections have an energy dependence that is broadly similar to the $\pi^+d \rightarrow pp$ reaction.

V. SUMMARY AND CONCLUSIONS

In this experiment, (π^+, pd) , and (π^+, dd) reactions were investigated using 100 and 165 MeV pion beams incident on ${}^{12}\text{C}$ and ${}^6\text{Li}$ targets, bringing to a close our investigation of the pion absorption reaction with discrete detectors

at TRIUMF. It was observed that the pd angular distributions were flatter than the pp distributions, and that the dd were the flattest of all. The two sets of distributions were offset from each other by nearly the same factor, indicating that the deuteron emission mechanism has the same origin in the two cases.

The pd , dp and dd kinematic distributions were compared with two empirical models. The first model, based on a parameterization of the full excitation spectrum of our earlier published [14] $^{12}\text{C}(\pi^+, pp)$ data, was termed ‘pp-like’ emission, as it assumes that the deuteron emission energy and angle distributions mirror those of proton emission. This could either be due to direct deuteron emission following π^+ absorption, deuteron knockout via ISI, or neutron pickup following a soft FSI. The second model, which included $^{12}\text{C}(p, d)^{11}\text{C}_{g.s.}$ cross sections as one of its inputs, simulated neutron pickup following pp emission via a hard FSI. The two mechanisms were fit to the data, with a common normalization factor for each mechanism at each of the two incident pion energies studied, independent of proton or deuteron emission angle. It was found that the appropriately normalized sum of the two mechanisms were able to describe all of the features of the data in an acceptable manner, and that nearly all of the observed yield for forward protons in coincidence with forward deuterons was due to neutron pickup. The importance of this mechanism increased with energy, possibly due to the increasing multiplicity of the underlying π^+ absorption reaction. Signatures of deuteron emission following direct quasi-triton absorption were also investigated, and were only found to play a substantive role at $T_\pi = 100$ MeV.

It is now known that the mechanisms contributing to pion absorption are even more complex than originally anticipated [11,14], so the clean identification of the role of FSI in such reactions remains a difficult task. The kinematic signatures of hard FSI are not distinctive, and occupy regions of phase-space already populated by other complex absorption mechanisms. Fortunately, however, neutron pickup has a distinctive experimental signature, and it is highly likely that it is one of the many possible hard final-state interactions following absorption. This work reaffirms the significant role played by FSI in hadronic interactions, and our success in quantitatively reproducing the shapes of the experimental distributions in terms of the $p-n$ pickup mechanism leads one to optimistically expect that the role of FSI in pion absorption reactions will ultimately be understood in much better detail than at present. FSI, of course, are not only important in hadron-induced reactions, but also in electron and photon-induced reactions. The issue of modeling other FSI, such as NN rescattering in all such reactions, could be revisited using a semi-empirical approach similar to that used here.

VI. ACKNOWLEDGEMENTS

We would like to thank S. Rusaw and M. Jackson for assisting in the analysis. This project was supported in part by the Natural Sciences and Engineering Research Council of Canada (NSERC), and the Saskatchewan Department of Economic Development. The generous assistance of E.W. Vogt, then Director of TRIUMF, is also gratefully acknowledged.

^(a) Present Address: Department of Physics, University of Ioannina, GR-45110 Ioannina, Greece

[1] D. Ashery, J.P. Schiffer, *Ann. Rev. Nucl. Part. Sci.* **36** (1986) 207.

[2] D. Androic, et al., *Phys. Rev. C* **53** (1996) R2591.

G. Backenstoss, et al., *Phys. Lett. B* **379** (1996) 60.

[3] J.C. Comiso, et al., *Phys. Lett.* **78B** (1978) 31.

[4] W.R. Wharton, et al., *Phys. Rev. C* **33** (1986) 1435.

[5] H. Yokota, et al., *Phys. Lett. B* **175** (1986) 23.

[6] H. Yokota, et al., *Phys. Rev. C* **39** (1989) 2090.

[7] R.D. Ransome, et al., *Phys. Rev. C* **42** (1990) 1500.

[8] R.D. Ransome, et al., *Phys. Rev. C* **45** (1992) R509.

[9] Th.S. Bauer, et al., *Phys. Rev. C* **46** (1992) R20.

[10] D. Rowntree, et al., *Phys. Rev. C* **60** (1999) 054610.

[11] A. Lehmann, et al., *Phys. Rev. C* **55** (1997) 2931.

[12] Z. Papandreou, et al., *Phys. Rev. C* **51** (1995) R2862.

[13] G.J. Lolos, et al., *Phys. Rev. C* **54** (1996) 211.

[14] G.M. Huber, et al., *Nucl. Phys. A* **624** (1997) 623.

- [15] Z. Papandreou, G.J. Lolos, G.M. Huber and X. Aslanoglou, Nucl. Instr. Meth. **A268** (1988) 179.
- [16] Z. Papandreou et. al., Nucl. Instr. Meth. **B34** (1988) 454.
- [17] T.J. Gooding and H.G. Pugh, Nucl. Instr. Meth. **7** (1960) 189.
- [18] N.S.Chant, P.S.Fisher, D.K.Scott, Nucl. Phys. **A99** (1967) 669.
- [19] H.Ohnuma et al., J. Phys. Soc. Jpn. **48** (1980) 1812.
- [20] P.G.Roos, et al., Nucl. Phys. **A255** (1975) 187.
- [21] CERN Computer Library W 505, 1977.
- [22] J.K.P.Lee, et al., Nucl. Phys. **A106** (1968) 357.
- [23] D. Bachelier, et al., Nucl. Phys. **A126** (1969) 60.
- [24] J. Kallne, E. Hagberg, Phys. Scr. **4** (1971) 151.
- [25] R. Hamers, Ph.D. thesis, Free University of Amsterdam, 1988, unpublished.
- [26] B.G. Ritchie, Phys. Rev. C **44** (1991) 533.
- [27] B.J. VerWest and R.A. Arndt, Phys. Rev. C **25** (1982) 1979.